miR-451 protects against erythroid oxidant stress by repressing 14-3-3ζ

Duonan Yu,[1,9] Camila O. dos Santos,[1,9,10] Guowei Zhao,[1,9] Jing Jiang,[1] Julio D. Amigo,[2] Eugene Khandros,[1] Louis C. Dore,[3] Yu Yao,[1] Janine D'Souza,[1] Zhe Zhang,[4] Saghi Ghaffari,[5] John Choi,[6] Sherree Friend,[7] Wei Tong,[1] Jordan S. Orange,[8] Barry H. Paw,[2] and Mitchell J. Weiss[1,11]

[1]Division of Hematology, The Children's Hospital of Philadelphia, Philadelphia, Pennsylvania 19104, USA; [2]Division of Hematology, Department of Medicine, Brigham and Women's Hospital, Harvard Medical School, Boston, Massachusetts 02115, USA; [3]Integrated Graduate Program, Feinberg School of Medicine, Northwestern University, Chicago, Illinois 60611, USA; [4]Center for Biomedical Informatics, The Children's Hospital of Philadelphia, Philadelphia, Pennsylvania 19104, USA; [5]Department of Gene and Cell Medicine, Mount Sinai School of Medicine, New York, New York, USA; [6]Department of Pathology, The Children's Hospital of Philadelphia, Philadelphia, Pennsylvania 19104, USA; [7]Amnis Corporation, Seattle, Washington 98121, USA; [8]Division of Immunology, The Children's Hospital of Philadelphia, Philadelphia, Pennsylvania 19104, USA

The bicistronic microRNA (miRNA) locus *miR-144/451* is highly expressed during erythrocyte development, although its physiological roles are poorly understood. We show that *miR-144/451* ablation in mice causes mild erythrocyte instability and increased susceptibility to damage after exposure to oxidant drugs. This phenotype is deeply conserved, as miR-451 depletion synergizes with oxidant stress to cause profound anemia in zebrafish embryos. At least some protective activities of miR-451 stem from its ability to directly suppress production of 14-3-3ζ, a phospho-serine/threonine-binding protein that inhibits nuclear accumulation of transcription factor FoxO3, a positive regulator of erythroid anti-oxidant genes. Thus, in *miR-144/451*$^{-/-}$ erythroblasts, 14-3-3ζ accumulates, causing partial relocalization of FoxO3 from nucleus to cytoplasm with dampening of its transcriptional program, including anti-oxidant-encoding genes *Cat* and *Gpx1*. Supporting this mechanism, overexpression of 14-3-3ζ in erythroid cells and fibroblasts inhibits nuclear localization and activity of FoxO3. Moreover, shRNA suppression of 14-3-3ζ protects *miR-144/451*$^{-/-}$ erythrocytes against peroxide-induced destruction, and restores catalase activity. Our findings define a novel miRNA-regulated pathway that protects erythrocytes against oxidant stress, and, more generally, illustrate how a miRNA can influence gene expression by altering the activity of a key transcription factor.

[*Keywords*: MicroRNA; erythropoiesis; FoxO3; hemolytic anemia]

Supplemental material is available at http://www.genesdev.org.

Received April 26, 2010; revised version accepted June 15, 2010.

Tissue development is controlled by nuclear factors that coordinate lineage-specific programs of gene expression. In addition to regulating protein-coding genes, transcription factors also specify the production of microRNAs (miRNAs), small noncoding RNAs that typically inhibit protein production by binding the 3′ untranslated region (UTR) of specific target mRNAs via imperfect Watson-Crick base-pairing (for reviews, see Bartel 2004; Ambros 2008; Carthew and Sontheimer 2009). This interaction recruits the RNA-induced silencing complex (RISC) of proteins that promote nucleolytic cleavage and/or inhibit translation of target mRNAs. miRNAs were discovered initially in *Caenorhabditis elegans*, and, soon thereafter, were found to be highly conserved throughout metazoan evolution. It is estimated that vertebrate genomes encode ~1000 miRNAs that are expressed in unique tissue and developmental-specific patterns. By regulating protein production post-transcriptionally, miRNAs influence the formation and function of most or all tissues. In addition, some miRNAs act as oncogenes or tumor suppressors. However, the regulation of most miRNAs and their precise mechanisms of action are not known. Numerous transcription factors and extensive post-transcriptional processing regulate miRNA synthesis. Moreover, most miRNAs have many targets, and most mRNAs are potentially regulated by more than one miRNA. Thus, miRNAs represent a complex and powerful mechanism for orchestrating

[9]These authors contributed equally to this work.
[10]Present address: Cold Spring Harbor Laboratory, 1 Bungtown Road, Cold Spring Harbor, NY 11724, USA.
[11]Corresponding author.
E-MAIL weissmi@email.chop.edu; FAX (215) 590-4834.
Article is online at http://www.genesdev.org/cgi/doi/10.1101/gad.1942110.

protein synthesis. One method to study the function of specific mammalian miRNAs is to delete the corresponding genes in mice, although relatively few have been studied in this manner.

Several lines of evidence indicate that miRNAs regulate red blood cell production (erythropoiesis), a topic of relevance to developmental hematopoiesis and the pathophysiology of human anemias. For example, hematopoietic-specific ablation of Argonaut 2 (*Ago2*), a RISC component, causes severe anemia and impaired erythropoiesis (O'Carroll et al. 2007). miR-24 inhibits erythropoiesis by repressing production of the activin type I receptor ALK4 (Wang et al. 2008). miR-221 and miR-222 modulate erythroid maturation by down-regulating c-Kit, the cytokine receptor for stem cell factor (SCF, kit ligand) (Felli et al. 2005). Despite these advances, comprehensive understanding of how miRNAs control erythropoiesis and erythrocyte functions is lacking.

Recently, we reported that the essential erythroid transcription factor GATA-1 directly activates a bicistronic miRNA locus encoding miR-144 and miR-451 (Dore et al. 2008). These miRNAs are strongly induced during zebrafish, mouse, and human erythroid maturation (Bruchova et al. 2007; Choong et al. 2007; Masaki et al. 2007; Zhan et al. 2007; Dore et al. 2008; Merkerova et al. 2008; Du et al. 2009; Fu et al. 2009; Pase et al. 2009; Papapetrou et al. 2010). miR-451 is also present in mature circulating red blood cells (Kloosterman et al. 2006; Rathjen et al. 2006). Overexpression of miR-451 augments chemical-induced maturation of murine erythroleukemia (MEL) cells. Conversely, miR-451/miR-144 antagonists inhibit erythroid maturation in MEL cells, in hematopoietic stem cells reintroduced into mice (Papapetrou et al. 2010), and in zebrafish embryos (Dore et al. 2008; Du et al. 2009; Pase et al. 2009). In zebrafish, miR-451 targets mRNA encoding transcription factor gata2 (Pase et al. 2009), and miR-144 regulates the production of embryonic α-globin indirectly by inhibiting klfd, a Kruppel-like DNA-binding protein (Fu et al. 2009; Du et al. 2009). However, these pathways are not completely conserved in mammals, and the overall function of the *miR-144/451* locus in erythropoiesis is not known for any organism.

To better define the functions of *miR-144/451*, we deleted the DNA-coding regions of both miRNAs in mice. At baseline, this mutation causes mild erythrocyte instability with hemoglobin precipitates (Heinz bodies), and expansion of erythroid precursors in the bone marrow and spleen. Moreover, loss of *miR-144/451* exacerbates the deleterious effects of oxidative stress on erythroid cells. Transcriptome analysis of mutant erythroblasts indicates that *miR-144/451* regulates the expression of many genes. The current study focuses on mechanisms by which miR-451 protects erythroid cells against oxidant injury. Specifically, miR-451 directly targets *Ywhaz* mRNA, which encodes the phospho-serine/threonine-binding protein 14-3-3ζ. Loss of miR-451 causes abnormal buildup of 14-3-3ζ, which in turn inhibits the activity of transcription factor FoxO3 by partially suppressing its nuclear localization. This impairs the expression of numerous FoxO3-regulated genes, including anti-oxidant enzymes. Our findings illustrate a new miRNA-regulated pathway that protects erythroid cells from oxidant stress.

Results

Erythroid abnormalities in miR-144/451$^{-/-}$ mice

To examine the role of miR-144 and miR-451 in murine erythroid development, we deleted a contiguous gene segment encoding both miRNAs (Supplemental Fig. 1). Homozygous null animals were born at a normal Mendelian ratio (Supplemental Table 1), bred normally, and displayed no obvious physical abnormalities. Mature miR-451 was undetectable in spleen and bone marrow of homozygous null animals (Supplemental Fig. 1C; data not shown).

Automated hematology analysis of *miR-144/451$^{-/-}$* mice revealed mild anemia and reticulocytosis with increased red cell distribution width (RDW), reflecting size variation (Table 1). No abnormalities in white blood cell or platelet counts were observed (data not shown). Blood smears of mutant mice showed polychromasia, indicating young red blood cells, with erythrocyte shape irregularities and occasional inclusions (Fig. 1A, left panels). Heinz bodies, reflecting precipitated hemoglobin, were present in *miR-144/451$^{-/-}$* erythrocytes (Fig. 1A, right panels), similar to what was observed after global hematopoietic inhibition of miRNA processing by ablation of *Ago2* (O'Carroll et al. 2007). Levels of α-globin and β-globin mRNAs were not altered in mutant erythroblasts (Fig. 3B, below). Membrane-associated globins in circulating knockout erythrocytes were very mildly increased, with α and β present in equal proportion (data not shown). These data indicate that the Heinz bodies are not caused by globin chain imbalance.

The spleens from *miR-144/451$^{-/-}$* mice were enlarged about twofold (Fig. 1B). Histology showed erythroid hyperplasia that was mild in the bone marrow and more marked in the spleen (Supplemental Fig. 2). In both tissues, there was mild to moderate accumulation of large immature erythroid precursors relative to smaller, more mature erythroblasts. However, flow cytometry

Table 1. *Erythrocyte indices of wild-type (+/+) and miR-144/451$^{-/-}$ mice (ages 6–10 wk)*

Index	+/+	–/–	*P*-value (*t*-test)	*n* (+/+)/(–/–)
RBC (m/μL)	10.10 ± 0.46	10.78 ± 0.57	0.006555	11/11
Hb (g/dL)	14.90 ± 0.44	14.27 ± 0.60	0.011314	11/11
HCT (%)	52.14 ± 2.72	50.41 ± 2.26	0.1209	11/11
MCV (fl)	51.61 ± 2.01	46.82 ± 1.94	0.000014	11/11
MCH (pg)	14.76 ± 0.58	13.26 ± 0.46	0.000001	11/11
RDW (%)	18.19 ± 1.09	20.55 ± 0.71	0.000007	11/11
Retic (%)	1.77 ± 0.22	2.97 ± 0.40	0.0001	6/6

(RBC) Erythrocyte count; (Hb) hemoglobin concentration; (HCT) hematocrit; (MCV) mean corpuscular volume; (MCH) mean corpuscular hemoglobin; (Retic) reticulocyte count. All values are shown as mean ± standard deviation.

analysis of bone marrow (Supplemental Fig. 3) and spleen (Supplemental Fig. 4) showed similar distributions of the erythroid developmental stage markers CD71, Ter119, and forward scatter (FSC) (Socolovsky et al. 2001; Liu et al. 2006) in wild-type and mutant tissues. The reasons for these differences between flow cytometry and histological data are unclear. It is possible that immature mutant erythroblasts are relatively fragile and preferentially lysed by collection and processing for flow cytometry. Regardless, our overall findings suggest that loss of *miR-144/451* induces mild destruction of circulating erythrocytes and expansion of precursor compartments in the bone marrow and, to a greater extent, in the spleen.

miR-144/451 *protects against oxidant stress*

We examined how loss of *miR-144/451* affects responses to erythroid stress by treating mice with phenylhydrazine (PHZ), an oxidant that induces denaturation of hemoglobin, resulting in rapid erythrocyte destruction (hemolysis). Compared with wild-type littermates, *miR-144/451*$^{-/-}$ mice exhibited more rapid and profound decreases in hematocrit levels and subsequent delayed recovery (Fig. 1C). The greater decline in hematocrit within the first few days after PHZ reflects enhanced hemolysis of mutant erythrocytes. The delayed recovery suggests that mutant erythroid precursors mature abnormally and/or are more susceptible to PHZ-induced injury. Upon exposure to hydrogen peroxide (H_2O_2), a physiological reactive oxygen species (ROS) precursor, *miR-144/451*$^{-/-}$ erythrocytes exhibited increased accumulation of ROS (Fig. 1D) and enhanced lysis (Fig. 1E) compared with controls. Moreover, the activity of catalase, a key H_2O_2-degrading enzyme, was reduced by ~50% in the mutant cells (Fig. 1F). In methylcellulose colony assays, the formation of burst-forming unit erythroid (BFU-e)-type colonies from mutant bone marrow progenitors was inhibited selectively by buthionine sulfoximine (BSO), a pro-oxidant that depletes cells of glutathione (Fig. 1G). In contrast, sensitivity to inhibition by BSO was similar in granulocyte–macrophage colonies from wild-type and *miR-144/451*$^{-/-}$ hematopoietic progenitors (data not shown). Together, these findings indicate that the *miR-144/451* gene protects erythroid cells against oxidant stress.

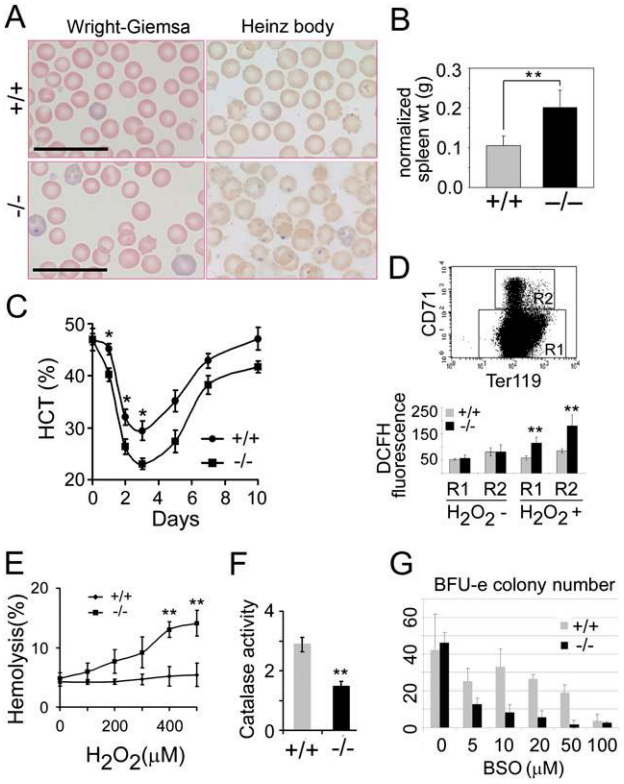

Figure 1. Baseline erythroid abnormalities and enhanced susceptibility to oxidative stress in *miR-144/451*$^{-/-}$ mice. (*A*) Erythrocyte morphology of wild-type (+/+) and *miR-144/451*$^{-/-}$ mice. The *left* panels show Wright-Giemsa stain. Mutant erythrocytes exhibit increased polychromasia (blue tinge) indicating young cells, variations in size and shape, and occasional inclusions. The *right* panels show Heinz body staining with methyl violet, which detects precipitated hemoglobin. Original magnification, 1000×; bars, 20 μm. (*B*) Splenomegaly in mutant mice. The *Y*-axis shows spleen weight normalized to body weight in 3- to 6-mo-old mice. (+/+) $n = 33$; (–/–) $n = 30$. (**) *P*-value < 0.01 (*t*-test). (*C*) Increased hemolysis of mutant erythrocytes after exposure to the oxidant PHZ. *miR-144/451*$^{-/-}$ mice ($n = 8$) and wild-type littermates ($n = 13$) were treated with PHZ (180 mg/kg) on days 0 and 1. Serial hematocrit determinations were performed after sampling 20 μL of blood from the tail vein. Data represent the average of three independent experiments. Error bars indicate standard error of the mean (SEM). (*) *P*-value < 0.05 (*t*-test). (*D*) Increased production of ROS in mutant erythroid cells after exposure to H_2O_2. (*Top* panel) Peripheral blood was stained with cell surface markers to identify mature erythrocytes (Ter119$^+$/CD71$^-$, R1) and reticulocytes (Ter119$^+$/CD71$^+$, R2). The cells were incubated with H_2O_2 and ROS were measured by flow cytometry using the fluorescent indicator 2′,7′-dichlorofluorescin (DCFH). $n = 6$ mice of each genotype. (**) *P*-value < 0.01 (*t*-test). (*E*) Increased sensitivity of erythrocytes to lysis by H_2O_2. Erythrocytes were incubated overnight in the indicated concentrations of H_2O_2. The extent of hemolysis is approximated by release of free hemoglobin, as measured by OD_{540} after removal of intact erythrocytes by centrifugation. Data represents the average of two independent experiments. $n = 4$ mice of each genotype. (**) *P*-value < 0.01 (*t*-test). (*F*) Reduced catalase activity in mutant erythrocytes compared with age-matched controls. Relative catalase activities from equal numbers of erythrocytes are shown. (+/+) $n = 8$; (–/–) $n = 11$. (**) *P*-value < 0.01 (*t*-test). (*G*) Mutant erythroid colony formation is inhibited by oxidant stress. Bone marrow cells were seeded into methylcellulose cultures containing erythropoietin, SCF, and the pro-oxidant BSO at the indicated concentrations. BFU-e colonies were enumerated 10 d later. The *Y*-axis shows number of BFU-e per 1.5×10^6 bone marrow cells.

Loss of miR-451 enhances oxidant-induced anemia in zebrafish

Previously, we reported that morpholino (MO)-induced knockdown of miR-451 causes profound anemia in zebrafish embryos (Dore et al. 2008). These experiments were performed in the presence of 1-phenyl-2-thiourea (PTU),

a tyrosinase inhibitor that blocks melanin synthesis to facilitate visualization of internal embryo structures (Karlsson et al. 2001). PTU contains a free thiol group capable of electron capture, and induces oxidant stress in several experimental systems (Das and Chainy 2004; Bonfigli et al. 2006; Zamoner et al. 2008). In light of the current findings in mice, we compared the effects of miR-451 MO with and without PTU on zebrafish erythropoiesis. miR-451 MO synergized with PTU to induce profound anemia, while either treatment alone had minimal effects (Fig. 2A; Supplemental Fig. 5A). Addition of the anti-oxidant N-acetyl cysteine (NAC) largely restored accumulation of erythroid cells in PTU-treated miR-451 morphants (Fig. 2B; Supplemental Fig. 5B). *cyp1a1* mRNA, known to be induced by PTU treatment (Wang et al. 2004) and oxidative stress (Wu et al. 2009), was increased significantly in PTU-treated morphants compared with treatment with PTU alone (Fig. 2C). Thus, in zebrafish embryos, PTU synergizes with miR-451 deficiency to potentiate oxidant stress and induce anemia. Accordingly, anti-oxidant activities of miR-451 are conserved in mice and zebrafish.

FoxO3-regulated activity is inhibited in miR-144/451$^{-/-}$ *mice*

To investigate the effects of *miR-144/451* on erythropoiesis, we compared the transcriptomes of wild-type and mutant bone marrow erythroblasts (Fig. 3). We purified cells according to expression of developmental markers CD71, Ter119, and FSC (Fig. 3A; Liu et al. 2006), and compared mRNA transcripts in identical populations (Ter119^{+}/CD71^{+}/FSC^{high}) from three mice of each genotype using the Affymetrix GeneChip Mouse Genome 430 2.0 Array, which interrogates ~16,000 unique genes. Most (15 out of 17) erythroid marker genes, including α-globin and β-globin, were expressed similarly in wild-type and mutant cells, indicating that the samples were of similar developmental stages (Fig. 3B). Overall, 1037 mRNA transcripts differed significantly (SAM *P*-value, <0.01) in expression between wild-type and mutant cells. 3′UTR matches to the seed sequence of miR-144 or miR-451, calculated as described previously (Dore et al. 2008), are relatively enriched for transcripts that are up-regulated in mutant erythroblasts compared with genes that are unchanged or down-regulated. Specifically, miR-451 seed sequence matches are present in 27out of 660 (4.1%) up-regulated mRNAs compared with 188 out of 15,285 (1.2%) of mRNAs that are repressed or unchanged (odds ratio = 3.42; *P* = 2.7e-7). Likewise, miR-144 seed sequence matches are present in 16 out of 660 (2.4%) up-regulated mRNAs compared with 190 out of 15,285 (1.2%) of mRNAs that are repressed or unchanged (odds ratio, 1.97; *P* = 0.02). Only 140 transcripts differed more than twofold between wild-type and mutant erythroblasts, consistent with the general concept that miRNAs produce many relatively small changes in gene expression to fine-tune tissue development or physiology (Lim et al. 2005; Flynt and Lai 2008). Analysis of differentially expressed transcripts using the database for annotation, visualization, and integrated discovery (DAVID) (Dennis et al. 2003) revealed alteration of numerous Gene Ontology categories (Supplemental Table 2), suggesting that loss of *miR-144/451* affects multiple aspects of erythropoiesis.

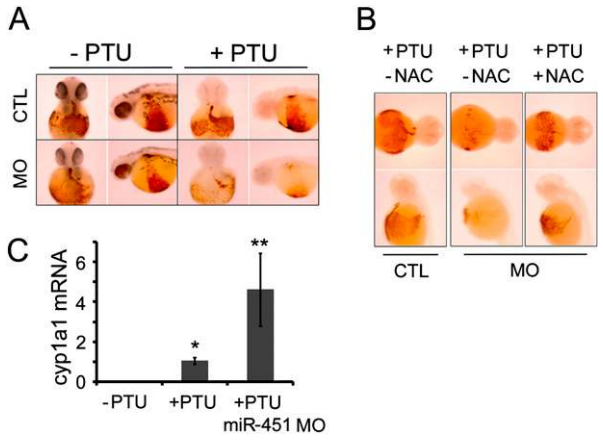

Figure 2. Increased oxidative stress and anemia in miR-451-depleted zebrafish embryos exposed to PTU. (*A*) One-cell stage fertilized embryos were injected with miR-451 MO, incubated with or without PTU and stained for hemoglobin with o-dianisidine at 48 h post-fertilization (hpf). (CTL) Uninjected control embryos. Similar results in multiple embryos are shown in Supplemental Figure 5A. (*B*) Zebrafish embryos were treated with various combinations of PTU, miR-451 MO, and the anti-oxidant NAC, then stained for hemoglobin at 48 hpf. Note that NAC reverses the anemia caused by PTU + miR-451 MO. Similar results in multiple embryos are shown in Supplemental Figure 5B. (*C*) Real-time RT–PCR showing the relative mRNA level of *cyp1a1*, a marker for oxidative stress, in total embryos after the indicated treatments. (*) *P*-value < 0.05; (**) *P*-value < 0.01 (*t*-test).

We used the transcriptome study to investigate susceptibility to oxidant stress conferred by loss of *miR-144/451*. We focused on the activity of transcription factor FoxO3 for several reasons. First, FoxO3 is a master regulator of anti-oxidant responses in numerous tissues, including erythroid (Kops et al. 2002; Marinkovic et al. 2007; Tan et al. 2008). Second, catalase (*Cat*) and glutathione peroxidase 1 (*Gpx1*), which are directly regulated by FoxO3 (Nemoto and Finkel 2002; Marinkovic et al. 2007; Tan et al. 2008), are repressed in *miR-144/451*$^{-/-}$ erythroid cells (Figs. 1F, 3F). Third, miR-451 targets *Ywhaz*, which encodes 14-3-3ζ, a phospho-serine/threonine-binding protein that negatively regulates FoxO3 activity (Brunet et al. 1999). Of 18 known FoxO3 target genes, nine were repressed (SAM, *P* < 0.07) in *miR-144/451*$^{-/-}$ erythroblasts (Fig. 3C). Overall, these FoxO3 targets were significantly more repressed than 17 erythroid marker genes, indicating that the altered FoxO3 program is not simply due to differences in the developmental stages of the wild-type versus *miR-144/451*$^{-/-}$ erythroblast populations analyzed (Fig. 3D).

We next examined how loss of *miR-144/451* affects the regulation of 299 genes whose expression was altered by induced FoxO3 activity in murine erythroblasts (Bakker

et al. 2007). Our microarray data included 222 of these genes (50 up-regulated and 172 down-regulated by FoxO3) (Fig. 3E). In general, erythroid genes that were demonstrated previously to be FoxO3-induced were repressed in *miR-144/451*$^{-/-}$ erythroblasts. Conversely, FoxO3-repressed genes tended to be up-regulated by loss of *miR-144/451* (Fig. 3E). Overall, our transcriptome analysis indicates that loss of *miR-144/451* impairs the activity of FoxO3, which positively regulates anti-oxidant responses in erythroid cells.

Of note, the microarray findings may underestimate the extent of FoxO3 dysregulation. We profiled FSC^{high}/Ter119^{+}/CD71^{+} erythroblasts, a developmental stage reflecting the onset of most FoxO3 activity during erythropoiesis (Marinkovic et al. 2007). It is possible that the effects of FoxO3 impairment increase at later stages of erythroid maturation in the mutant animals. In support, the FoxO3-regulated anti-oxidant gene *Cat* (encoding catalase) is down-regulated to a lesser extent in *miR-144/451*$^{-/-}$ FSC^{high}/Ter119^{+}/CD71^{+} bone marrow erythroblasts compared with the total Ter119^{+} population of mutant cells, which contains more mature erythroid precursors (Fig. 3C,F). Another FoxO3 target, *Gpx1*, is expressed normally in mutant FSC^{high}/Ter119^{+}/CD71^{+} erythroblasts, but is reduced by ~40% in the total Ter119^{+} population. These differences are not likely due to nonspecific alterations in cellular maturation, since wild-type and mutant Ter119^{+} erythroblasts exhibited similar distributions of developmental stage markers both before (Supplemental Fig. 3) and after immunomagnetic bead selection (data not shown). Also note that some FoxO3-regulated genes are not repressed in mutant erythroblasts (Fig. 3C,E,F). This probably reflects partial reduction of FoxO3 with varying dosage requirements at specific target genes (discussed in the next section).

Reduced nuclear accumulation of FoxO3 in miR-144/451$^{-/-}$ *erythroblasts*

We investigated how FoxO3 activity might be altered by loss of *miR-144/451*. *FoxO3* mRNA and protein levels are similar in mutant erythroblasts compared with a stage-matched population of wild-type control cells (Fig. 4A,B). The activity of FoxO3 is modulated largely through regulated subcellular localization that occurs in response

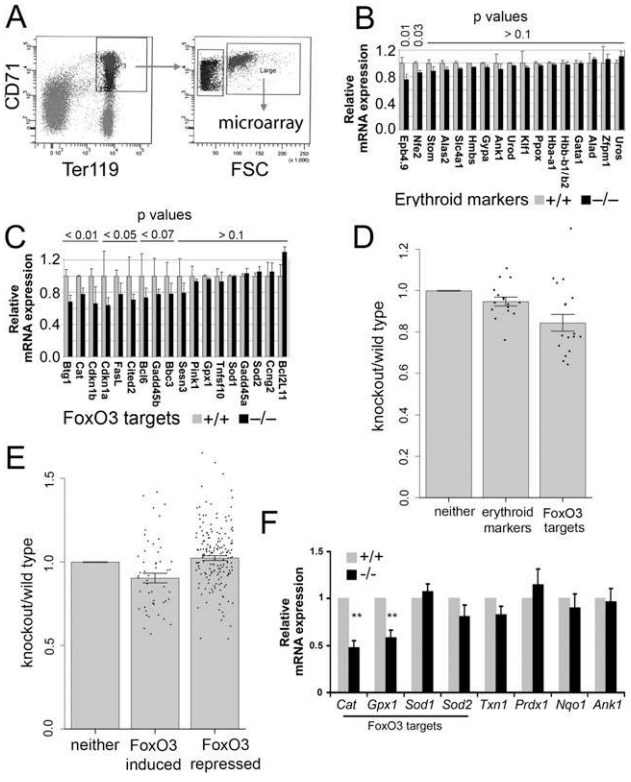

Figure 3. Loss of *miR-144/451* inhibits FoxO3-regulated gene expression in erythroblasts. (*A*) Microarray transcriptome analysis. Bone marrow erythroblasts were fractionated according to the developmental markers Ter119, CD71, and FSC. Stage-matched Ter119^{+}/CD71^{+}/FSC^{HI} erythroblasts from wild-type (wt) and *miR-144/451*$^{-/-}$ mice were analyzed for mRNA expression using Affymetrix GeneChips. (*B*) Microarray data from three *miR-144/451*$^{-/-}$ and three wild-type (+/+) mice were analyzed for the expression of 17 erythroid marker genes (*X*-axis). Relative expression levels are shown on the *Y*-axis with microarray signals from wild-type cells assigned a relative value of 1. *P*-values (*t*-test) are indicated at the *top* of the graphs. (*C*) Microarray data from three *miR-144/451*$^{-/-}$ and three wild-type (+/+) mice were analyzed for the expression of 18 FoxO3-activated target genes identified from literature searches (*X*-axis). Relative expression levels are shown on the *Y*-axis with microarray signals from wild-type cells assigned a relative value of 1. *P*-values (*t*-test) are indicated at the *top* of the graphs. (*D*) FoxO3 target genes (shown in *C*) were selectively repressed relative to erythrocyte marker genes (shown in *B*) in *miR-144/451*$^{-/-}$ erythroblasts. The plots show distribution of expression difference between wild-type and mutant mice for the categories indicated on the *X*-axis. The plot labeled "neither" reflects all erythroblast genes (n = 15,945), excluding the 17 erythroid markers and 18 FoxO3 targets analyzed in the other plots. Individual genes are marked as diamonds, with locations jittered horizontally to reduce overlapping. The *Y*-axis shows differential gene expression between wild-type and *miR-144/451*$^{-/-}$ erythroblasts. *P*-values (*t*-test): neither versus erythroid marker, 0.03; neither versus FoxO3 targets, 0.003; erythroid marker versus FoxO3 targets, 0.04. (*E*) Loss of miR-144/451 inhibits erythroid FoxO3 activity. The *X*-axis indicates genes that were induced (n = 50) or repressed (n = 172) after activation of FoxO3 in erythroid cells, according to a previous study (Bakker et al. 2007). The bar marked "neither" represents the entire cohort of expressed mRNAs detected in the current study minus FoxO3-induced and FoxO3-repressed genes detected by Bakker et al. (2007). The plots show the distribution of expression difference in erythroblasts from wild-type versus *miR-144/451*$^{-/-}$ mice for the categories indicated on the *X*-axis. Individual genes are marked as in *D*. The *Y*-axis shows differential gene expression between wild-type and *miR-144/451*$^{-/-}$ erythroblasts. *P*-values: neither versus FoxO3-induced, 0.003; neither versus FoxO3 repressed, 0.08. (*F*) Real-time RT–PCR analysis to quantify gene expression in wild-type and *miR-144/451*$^{-/-}$ Ter119^{+} erythroblasts. *Cat*, *Gpx1*, *Sod1*, and *Sod2* are FoxO3 targets. *Txn1*, *Prdx1*, and *Nqo1* are anti-oxidant genes not known to be regulated by FoxO3. A control mRNA, *Ank1*, encodes an erythrocyte membrane protein. (*) $P < 0.05$ (*t*-test).

to various stresses and cytokine signaling pathways (for review, see Huang and Tindall 2007). Therefore, we investigated whether loss of *miR-144/451* alters FoxO3 localization in erythroid cells.

We purified Ter119$^+$ splenic erythroblasts by magnetic bead selection, immobilized the cells on polylysine-coated glass slides, and examined FoxO3 subcellular localization by quantitative immunofluorescence confocal microscopy (Fig. 4C,D). Wild-type and mutant Ter119$^+$ erythroblasts used for this analysis exhibit similar CD71/Ter119/FSC profiles (Supplemental Fig. 4) and express similar levels of α-globin protein (Fig. 5B,C), indicating that they represent developmental stage-matched populations. In wild-type Ter119$^+$ erythroblasts, FoxO3 colocalized predominantly with the nuclear stain DAPI (Fig. 4C, top panels), as reported previously (Marinkovic et al. 2007). In contrast, *miR-144/451*$^{-/-}$ erythroblasts tended to exhibit increased cytoplasmic distribution of FoxO3 (Fig. 4C, bottom panels). Quantitative imaging analysis demonstrated that the nuclear:cytoplasmic ratio of FoxO3 immunostaining was reduced by approximately one-third in *miR-144/451*$^{-/-}$ erythroblasts relative to their wild-type counterparts (Fig. 4D).

The confocal immunofluorescence microscopy data indicated that loss of miR-144/451 inhibits nuclear accumulation of FoxO3. We sought to verify these findings using an independent method. We isolated total hematopoietic cells from bone marrow and stained them with antibodies against CD71 and Ter119. The cells were then fixed, permeabilized, and stained with an anti-FoxO3 antibody that recognizes a different epitope than the antibody used for confocal immunofluorescence microscopy. The stained cells were analyzed using an ImageStream, which performs simultaneous high-throughput flow cytometry and individual cell image acquisition to quantify the intensities and subcellular location of fluorescent probes (George et al. 2006). This allowed us to compare the nuclear:cytoplasmic distributions of FoxO3 staining in statistically significant numbers of stage-matched (Ter119$^+$ and CD71$^+$) erythroblasts derived from wild-type and *miR-144/451*$^{-/-}$ mice. Representative images and quantitative analysis are shown in Figure 4, E

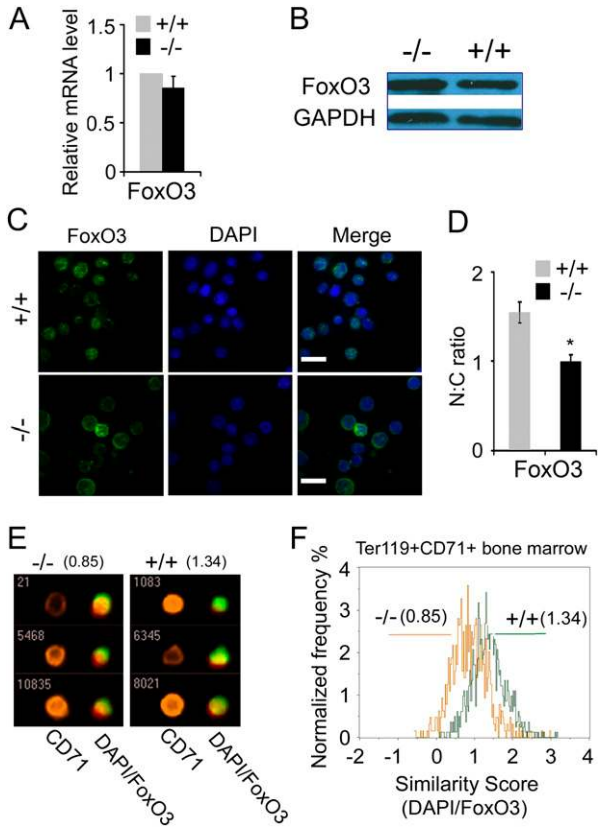

Figure 4. Reduced nuclear accumulation of FoxO3 protein in *miR-144/451*$^{-/-}$ erythroblasts. (A) Real-time RT–PCR quantification of *FoxO3* mRNA in Ter119$^+$ erythroblasts from *miR-144/451*$^{-/-}$ (−/−, n = 11) mice and wild-type (wt, +/+, n = 8) age-matched controls. Wild-type mRNA levels were assigned an arbitrary relative value of 1. The *Y*-axis shows relative expression. mRNA levels were normalized to those of *Gapdh*. (*B*) Western blot analysis of FoxO3 and GAPDH protein expression in Ter119$^+$ erythroblasts. Each lane represents 20 μg of protein extracted from whole cells. (*C*) Confocal immunofluorescence microscopy. Splenic Ter119$^+$ erythroblasts from *miR-144/451*$^{-/-}$ mice and wild-type littermate controls were immobilized onto poly-L-lysine-coated glass slides, fixed, and stained with anti-FoxO3 antibody, which was detected using a Cy2-conjugated secondary antibody (green). The nucleus was stained with DAPI (blue). Cells were imaged on a Zeiss spinning-disc confocal microscope with a 63× objective. Representative images are shown. Bar, 10 μm. (*D*) Quantitative image analysis of FoxO3 protein distribution from confocal microscopy images. The mean fluorescent intensity (MFI) of FoxO3 immunocytochemical signal was quantified in the nucleus and in whole cells using Volocity software. Cytoplasmic signal was calculated as the difference between whole-cell and nuclear MFI. The nuclear to cytoplasmic (N:C) FoxO3 MFI ratio is shown for each genotype. Approximately 200 cells were analyzed from four mice of each genotype. (*) P-value < 0.05 (t-test). (*E*) Subcellular localization of FoxO3 protein in primary erythroblasts using imaging flow cytometry. Bone marrow cells from *miR-144/451*$^{-/-}$ mice (−/−) and wild-type (+/+) age-matched controls were stained with Ter119, CD71, and FoxO3 antibodies and the nuclear stain DAPI, then analyzed using an Amnis ImageStream System model IS100, which performs simultaneous flow cytometry and quantitative image analysis on individual cells. Representative images of immunofluorescent staining are shown for Ter119$^+$CD71$^+$ cells from mice of each genotype. *Left* columns in both panels show CD71 staining at the cell surface. *Right* columns show staining for FoxO3 protein and DAPI. Numbers at the *top* of the panels indicate similarity scores, which reflect the extent to which the fluorescent signals from FoxO3 and nuclear DAPI coincide within each individual cell. The lower similarity score in *miR-144/451*$^{-/-}$ erythroblasts indicates reduced nuclear FoxO3. (*F*) Similarity score distribution for FoxO3 and DAPI in ~1000 Ter119$^+$/CD71$^+$ bone marrow erythroblasts from wild-type and *miR-144/451*$^{-/-}$ mice. The median similarity scores for each genotype are indicated in parentheses, with corresponding representative images shown in *E*. Lower similarity scores reflect decreased nuclear FoxO3 localization in the mutant erythroblasts. Representative data are shown; similar results were obtained from six mice of each genotype.

and F, respectively. Nuclear accumulation of FoxO3 was quantified using IDEAS image analysis software by calculating a similarity score of DNA and FoxO3 images (see the Supplemental Material). Figure 4F shows that the similarity score for FoxO3 and the nuclear stain DAPI is lower in *miR-144/451*$^{-/-}$ erythroblasts compared with controls, indicating reduced nuclear localization of FoxO3, in agreement with the confocal immunofluorescence studies. Similar results were obtained using spleen erythroblasts (data not shown). Thus, two independent experimental approaches using different antibodies show that loss of *miR-144/451* reduces nuclear accumulation of FoxO3.

miR-451 *targets* Ywhaz *mRNA to inhibit 14-3-3ζ protein expression*

The bioinformatic algorithm TargetScan (Lewis et al. 2005) identifies *Ywhaz/14-3-3ζ* mRNA as a potential miR-451 target. We noted that *Ywhaz/14-3-3ζ* is a potential effector of FoxO3 subcellular localization. Specifically, the AKT/PKB serine–threonine kinase phosphorylates FoxO3 on three conserved residues, which creates binding sites for the 14-3-3 family of adaptor proteins (for reviews, see Huang and Tindall 2007; Calnan and Brunet 2008). The resultant FoxO3:14-3-3 protein complex is shuttled to the cytoplasm, thereby inhibiting FoxO3 activity. In addition, 14-3-3ζ activates AKT by stimulating the formation of upstream cytokine signaling complexes (Barry et al. 2009). These prior findings raise the possibility that loss of miR-451 derepresses 14-3-3ζ protein production, which in turn inhibits FoxO3 activity by reducing its nuclear accumulation. Therefore, we investigated whether *miR-451* regulates 14-3-3ζ level.

miR-451 exhibits partial complementarity to the 3′UTR of *Ywhaz/14-3-3ζ* mRNAs of multiple species, particularly in the seed sequence region, an important determinant of miRNA–target mRNA interactions (Fig. 5A). Overexpression of miR-451 by retroviral transfer into two different erythroid lines, G1E and MEL, specifically reduced 14-3-3ζ protein expression (Supplemental Fig. 6A,B). Conversely, in *miR-144/451*$^{-/-}$ mice, 14-3-3ζ protein expression was increased by about sixfold and twofold in magnetic bead-purified Ter119^{+} erythroblasts from bone marrow (Fig. 5B; Supplemental Fig. 6C) and spleen (Fig. 5C; Supplemental Fig. 6C), respectively. Note that α-globin protein levels are similar in wild-type and mutant Ter119^{+} erythroblasts, indicating that the two populations are stage-matched. Thus, in erythroid cells, *Ywhaz*/14-3-3ζ protein expression correlates inversely with miR-451 levels.

Ywhaz is the only 14-3-3 mRNA up-regulated in *miR-144/451* erythroblasts (Supplemental Fig. 7A; Patrick et al. 2010). Western blot analysis using isoform-specific antibodies with recombinant protein standards shows

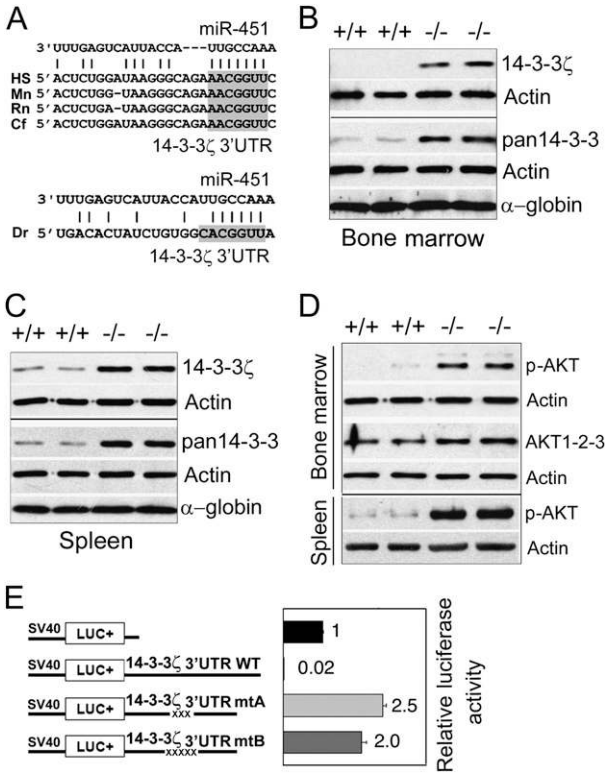

Figure 5. miR-451 targets *Ywhaz/14-3-3ζ* mRNA. (*A*) Multispecies nucleotide sequence alignments showing partial complementarity between the 3′UTRs of *Ywhaz/14-3-3ζ* mRNAs and miR-451. The miRNA seed sequence recognition sites in the mRNAs are boxed in gray. (Hs) Human; (Mn) mouse; (Rn) rat; (Cf) dog; (Dr) zebrafish. (*B*) Increased 14-3-3ζ and total 14-3-3 proteins in bone marrow *miR-144/451*$^{-/-}$ erythroblasts relative to wild-type (+/+) controls. Ter119^{+} cells were purified from bone marrow, and whole-cell lysates were analyzed by Western blotting with the indicated antibodies. The "pan" antibody recognizes all seven 14-3-3 isoforms, while the ζ antibody is isoform-specific (Supplemental Fig. 7B). Representative studies from two mice of each genotype are shown. Quantitative image analysis from multiple experiments are shown in Supplemental Figure 6C. (*C*) Increased 14-3-3ζ and total ("pan") 14-3-3 proteins in splenic *miR-144/451*$^{-/-}$ erythroblasts relative to wild-type (+/+) controls. Western blotting was performed as described for *B*. (*D*) Increased phosphorylation of AKT (S473) in *miR-144/451*$^{-/-}$ erythroblasts. Ter119^{+} cells were purified, and whole-cell lysates were analyzed by Western blot using the indicated antibodies. AKT1-2-3 indicates total AKT protein, while p-AKT indicates activated phosphorylated form. Representative results are shown from two mice of each genotype. (*E*) Interaction between *miR-451* and the 14-3-3ζ 3′UTR inhibits expression of a linked reporter gene. Firefly luciferase cDNA was fused to the normal 3′UTR of 14-3-3ζ cDNA or two mutant versions (mtA and mtB) containing 3-base-pair (bp) and 5-bp mutations within the region complementary to *miR-451* seed sequence. The reporter constructs were cloned into an expression vector and transfected into 293T cells along with a miR-451 expression construct and a constitutively active Renilla luciferase control plasmid. Luciferase activities were determined 24 h post-transfection. The bars in the *right* panel indicate firefly/Renilla luciferase activity, with levels from reporter vector lacking the 14-3-3ζ 3′UTR assigned an arbitrary value of 1. Numbers to the *right* of the bars indicate relative ratio of firefly luciferase activity. Results indicate the average of three separate experiments.

that 14-3-3ζ is the predominant isoform expressed in *miR-144/451*$^{-/-}$ erythroblasts (Supplemental Fig. 7B,C). Moreover, Western blot analysis using a "pan" antibody that recognizes all 14-3-3 isoforms roughly equally showed significant increase of total 14-3-3 protein in *miR-144/451*$^{-/-}$ erythroblasts, paralleling the findings obtained with the 14-3-3ζ isoform-specific antibody (Fig. 5B,C). Together, these findings indicate that total 14-3-3 activity is increased in the mutant erythroblasts via derepression of the ζ isoform. Increased phospho-AKT was present in *miR-144/451*$^{-/-}$ erythroblasts, consistent with prior studies showing that overexpressed 14-3-3ζ activates AKT (Fig. 5D; Brunet et al. 1999; Danes et al. 2008; Barry et al. 2009). In contrast, there was no accumulation of phospho-Stat-5 or ERK (data not shown). Thus, enhanced phospho-AKT accumulation is not likely due to overactive signaling from the erythropoietin receptor (EpoR).

To investigate further whether miR-451 regulates *Ywhaz/14-3-3ζ* mRNA directly, we linked the 3′UTR to the protein-coding region of luciferase cDNA, and transfected this reporter, along with the miR-451 expression construct, into 293T cells. Fusion of the *Ywhaz*/14-3-3ζ 3′UTR to luciferase cDNA decreased enzymatic activity in transfected cells by >50-fold, presumably reflecting decreased luciferase protein expression (Fig. 5E). This effect was abrogated by 3′UTR mutations that specifically inhibit interaction with the seed sequence of miR-451. Thus, miR-451 inhibits erythroid 14-3-3ζ protein expression by interacting directly with its mRNA.

Enforced expression of 14-3-3ζ inhibits nuclear accumulation and activity of FoxO3

We tested whether failure to repress 14-3-3ζ is sufficient to inhibit nuclear accumulation of FoxO3 during erythroid maturation. We used the MIGR1 retroviral vector to express a miR-451-resistant form of *Ywhaz/14-3-3ζ* cDNA in G1E-ER4 cells, a *Gata1*$^{-}$ erythroblast line that stably expresses a conditionally active GATA-1/estrogen receptor (ER) fusion protein (Fig. 6A; Gregory et al. 1999). When G1E-ER4 cells are treated with estradiol, GATA-1 becomes activated, triggering terminal erythroid maturation, as evidenced by characteristic changes in morphology and gene expression (Welch et al. 2004). In control G1E-ER4 cells, 14-3-3ζ protein decreased by about twofold to threefold at 36 h after GATA-1-induced maturation (Fig. 6A, lanes 1,2). This effect is due, at least in part, to the inhibitory effects of miR-451, which is strongly induced by GATA-1 (Supplemental Fig. 9A; Dore et al. 2008). In the absence of GATA-1 activity (no estradiol present), MIGR1-*Ywhaz*-transduced G1E-ER4 cells expressed higher levels of 14-3-3ζ compared with vector-transduced control cells (Fig. 6A, top panel, lanes 1,3), and the protein failed to be down-regulated after GATA-1 activation (Fig. 6A, top panel, lanes 3,4). Transduction with 14-3-3ζ-expressing retrovirus also increased total 14-3-3 protein detected by the "pan" antibody. Enforced expression of 14-3-3ζ did not impair miR-451 induction during erythroid maturation of G1E-ER4 cells (Supplemental Fig. 9A). We next examined how constitutively expressed 14-3-3ζ

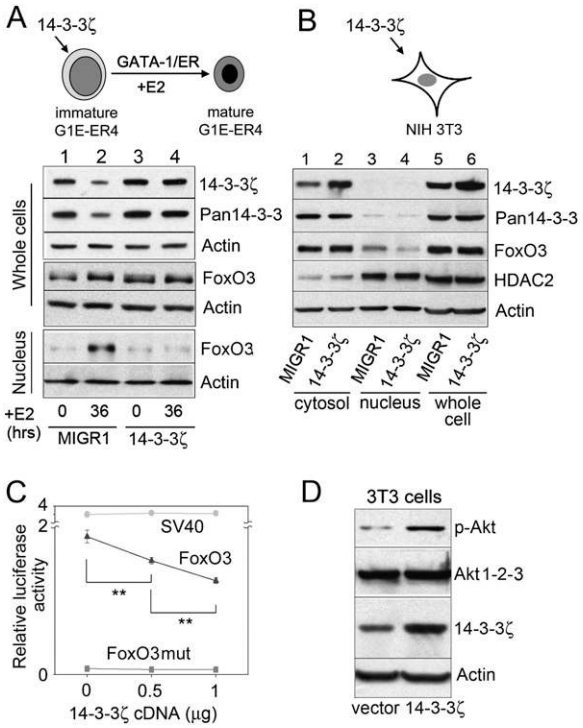

Figure 6. 14-3-3ζ regulates nuclear accumulation of FoxO3. (*A*) Enforced expression of 14-3-3ζ blocks nuclear accumulation of FoxO3 during erythroid maturation. G1E-ER4 is a *Gata1*$^{-}$ erythroblast line stably expressing GATA-1/ER. Treatment with estradiol (E2) activates GATA-1/ER, inducing terminal erythroid maturation. G1E-ER4 cells were infected with retrovirus encoding a miR-451-resistant 14-3-3ζ cDNA or empty control vector (MIGR1-puro). Pools of transduced cells were selected by treatment with puromycin. Western blot analysis was performed for the indicated proteins in whole-cell lysates and nuclear extracts at baseline and 36 h after estradiol-induced erythroid maturation. Note that FoxO3 normally redistributes to the nucleus upon erythroid maturation (nuclear expression in lanes *1,2*). This is inhibited by enforced expression of miR-451-resistant 14-3-3ζ. (Lanes *3,4*) Quantitative analysis of three independent experiments are shown in Supplemental Figure 9B. (*B*) 14-3-3ζ inhibits nuclear accumulation of FoxO3 in NIH3T3 cells. Cells were infected with retrovirus encoding miR-451-resistant 14-3-3ζ mRNA or MIGR1-puro empty vector. FoxO3 levels in nucleus and cytoplasm were analyzed by Western blot. HDAC2 and actin are loading controls. Quantitative analyses of three independent experiments are shown in Supplemental Figure 9C. (*C*) 14-3-3ζ inhibits FoxO3 activity. Reporter plasmids consisting of five wild-type (wt) or five mutant (mut) FoxO3-binding sites fused to firefly luciferase cDNA were transfected into NIH 3T3 cells along with a FoxO3 cDNA expression construct and varying amounts of 14-3-3ζ cDNA, as indicated on the *X*-axis. The SV40-luciferase reporter represents a FoxO3-independent control. Firefly luciferase activity was measured 36 h after transfection. Relative reporter activities normalized to the activity of a cotransfected Renilla luciferase control plasmid are indicated on the *Y*-axis. Data represent results from four independent experiments. (**) *P*-value < 0.01 (*t*-test). (*D*) Western blot showing increased activated (phospho)-Akt in 14-3-3ζ-overexpressing cells compared with vector-transduced cells. Similar results were obtained in four independent experiments.

affects nuclear localization of FoxO3. In vector-transduced G1E-ER4 cells, FoxO3 accumulated in the nucleus during GATA-1-induced maturation (Fig. 6A, bottom panel, lanes 1,2), similar to what occurs during erythroid maturation in vivo (Marinkovic et al. 2007). These Western blot findings were verified by ImageStream flow cytometry analysis (Supplemental Fig. 8). However, nuclear accumulation of FoxO3 during G1E-ER4 cell erythroid maturation was significantly inhibited by enforced expression of 14-3-3ζ (Fig. 6A, bottom panel, lanes 2,4; Supplemental Fig. 9B).

Enforced expression of 14-3-3ζ also altered FoxO3 nuclear localization in nonerythroid cells. NIH 3T3 cells infected with retrovirus encoding *Ywhaz*/14-3-3ζ expressed approximately twofold elevated 14-3-3ζ protein (Fig. 6B, lanes 1,2,5,6). Concomitantly, the level of nuclear FoxO3 protein was consistently reduced by ~50% (Fig. 6B, lanes 3,4; Supplemental Fig. 9C), while total cellular FoxO3 was unchanged (Fig. 6B, lanes 5,6). Next, we tested whether 14-3-3ζ levels affect FoxO3 transcriptional activity by using a reporter plasmid in which five FoxO3-binding sites are linked to a luciferase cDNA. This reporter was transfected into NIH 3T3 cells along with a FoxO3 cDNA expression plasmid, resulting in significant luciferase activity that was dependent on intact FoxO3-binding sites (Fig. 6C). Cotransfection of a 14-3-3ζ cDNA expression plasmid caused dose-dependent decreases in reporter activity, consistent with reduced FoxO3 nuclear localization demonstrated in Figure 6B. This effect was specific, as overexpressed 14-3-3ζ did not inhibit the expression of pSV40-luciferase, a FoxO3-independent reporter plasmid. Overexpressed 14-3-3ζ increased the level of phospho-(activated)-Akt (Fig. 6D; Supplemental Fig. 10), consistent with prior studies (Brunet et al. 1999; Danes et al. 2008; Barry et al. 2009) and our observation that Akt activation is increased in *miR-144/451*$^{-/-}$ erythroblasts (Fig. 5D).

Together, these studies show that mild (approximately twofold) overexpression of 14-3-3ζ protein is sufficient to partially inhibit FoxO3 nuclear accumulation both during erythroid maturation and in nonerythroid cells. This is consistent with our findings in primary *miR-144/451*$^{-/-}$ erythroblasts, which exhibit approximately twofold to sixfold elevated 14-3-3ζ (Fig. 5B,C; Supplemental Fig. 6C) and impaired accumulation of nuclear FoxO3 (Fig. 4).

shRNA knockdown of 14-3-3ζ confers resistance to oxidative stress, and restores catalase activity in miR-144/451$^{-/-}$ *erythrocytes*

We isolated hematopoietic stem/progenitor cells from *miR-144/451*$^{-/-}$ mice, infected them with retrovirus expressing shRNAs against either *Ywhaz/14-3-3ζ* mRNA or luciferase RNA as control, and transplanted them via intravenous injection into lethally irradiated *miR-144/451*$^{-/-}$ hosts (Fig. 7A). The retroviral vector also expressed GFP to track infected cells. Bone marrow erythroid progenitors expressing Ywhaz/14-3-3ζ shRNA exhibited ~80% reduction in the corresponding mRNA (Fig. 7B). Approximately 20%–30% of circulating erythrocytes were GFP$^+$, and therefore originated from retrovirally infected donor (*miR-144/451*$^{-/-}$) progenitors, while GFP$^-$ erythrocytes originated from uninfected donor cells or *miR-144/451*$^{-/-}$ host cells.

Mutant erythrocytes were hypersensitive to lysis after in vitro treatment with H_2O_2, as measured by a flow cytometry-based assay (Fig. 7C, far left panels), in agreement with data shown in Figure 1E. This phenotype was rescued specifically in erythrocytes derived from *miR-144/451*$^{-/-}$ progenitors transduced with Ywhaz/14-3-3ζ shRNA (Fig. 7C, graphs in middle and right panels). We used flow cytometry to fractionate erythrocytes derived from retrovirally infected *miR-144/451*$^-$ donor cells (GFP$^+$) from uninfected ones (GFP$^-$), and compared their levels of catalase activity. Knockdown of 14-3-3ζ in mutant hematopoietic progenitors increased catalase activity in mature erythrocyte progeny by ~60% relative to GFP$^-$ control cells from the same mice. In contrast, introduction of luciferase shRNA had no effect on catalase activity (Fig. 7D). Thus, reducing 14-3-3ζ expression in *miR-144/451*$^{-/-}$ hematopoietic progenitors enhanced erythrocyte resistance to H_2O_2 lysis and restored the activity of catalase, which derives from a key FoxO3 target gene.

Discussion

miR-144/451 is strongly induced during erythropoiesis in zebrafish, mice, and humans (Kloosterman et al. 2006; Choong et al. 2007; Masaki et al. 2007; Zhan et al. 2007; Dore et al. 2008; Du et al. 2009), and artificial manipulation of these miRNAs alters erythroid maturation in several experimental models (Zhan et al. 2007; Dore et al. 2008; Pase et al. 2009; Papapetrou et al. 2010). Here we report the consequences of *miR-144/451* ablation in mice, and further investigations into the effects of miR-451 depletion in zebrafish. In both instances, deficiencies of these miRNAs produced relatively mild erythroid phenotypes that were exacerbated upon exposure to oxidant drugs. These findings are consistent with the emerging concept that many mammalian miRNAs are not essential for tissue formation, but rather, fine-tune physiological functions and/or protect against various stresses (Li et al. 2007; van Rooij et al. 2007; Williams et al. 2009).

While this study was under review, two groups reported that processing of miR-451 precursor RNA is independent of Dicer, but requires Ago2 endonuclease activity (Cheloufi et al. 2010; Cifuentes et al. 2010). Mice homozygous for a missense mutation that inactivates Ago2 endonuclease express no mature miR-451, and die at birth with moderately severe anemia. Our current findings, along with those of Patrick et al. (2010), indicate that the relatively severe phenotype caused by loss of Ago2 endonuclease activity cannot be explained entirely by loss of miR-451, which at baseline causes only mild erythroid defects and no lethality. Thus, additional in vivo requirements for Ago2 catalytic activity must exist.

Our transcriptome data indicate that the *miR-144/451* gene modulates numerous cellular processes through multiple target mRNAs. Here we focus on a single important target gene and an associated signaling pathway that regulates, at least in part, the ability of miR-451

to protect against oxidant stress. Specifically, we show that miR-451 targets *Ywhaz/14-3-3ζ* mRNA to inhibit its expression. Loss of miR-451 causes 14-3-3ζ protein to accumulate in erythroid precursors, thereby activating AKT and impairing the transcriptional activity of FoxO3, a key positive regulator of anti-oxidant genes. AKT is responsive to many signals, and may also be activated in *miR-144/451*$^{-/-}$ erythroblasts through additional mechanisms that are 14-3-3-independent. It is also likely that derepressed 14-3-3ζ alters other aspects of erythropoiesis, given the interactions of this adaptor protein with multiple hematopoietic cytokine receptor signaling pathways (Stomski et al. 1999; Brummer et al. 2008; Barry et al. 2009). In agreement, Patrick et al. (2010), found that deregulated 14-3-3ζ expression inhibits erythroid maturation in fetal livers of *miR-451*$^{-/-}$ embryos. Patrick et al. (2010), also determined that loss of miR-451 alone confers susceptibility to PHZ-induced hemolysis, suggesting that this miRNA has the predominant role in protection against oxidant stress in the *miR-144/451*$^{-/-}$ mice described here. Together, our findings and those of Patrick et al. (2010) demonstrate that *Ywhaz/14-3-3ζ* is a key biologically relevant miR-451 target gene.

Erythroid cells are particularly sensitive to oxidant stresses and contain numerous relevant defenses, including FoxO3-regulated anti-oxidant enzymes (Marinkovic et al. 2007). In early-stage erythroid precursors, signaling via the Kit receptor and, to a lesser extent, the EpoR activate AKT, which phosphorylates FoxO3 (Bakker et al. 2004, 2007). This facilitates binding to 14–3–3 proteins, which inhibit FoxO3 activity by transporting it out of the nucleus (for review, see Huang and Tindall 2007). Sequential declines in Kit and EpoR signaling during normal erythroid maturation permit FoxO3 to enter the nucleus and activate its anti-oxidant program. Our current data demonstrate that miR-451 facilitates FoxO3 actions during terminal erythropoiesis by inhibiting the production of 14-3-3ζ. Overexpressed 14-3-3ζ, as observed upon loss of miR-451, could inhibit FoxO3 nuclear accumulation through at least two mechanisms (Fig. 7E). First, 14-3-3ζ binds phosphorylated FoxO3 to physically facilitate its nuclear export. Second, 14-3-3ζ promotes activation of AKT (Brunet et al. 1999; Danes et al. 2008; Barry et al. 2009), which in turn phosphorylates FoxO3 to create 14-3-3 docking sites. 14-3-3 proteins represent a family of seven related members that bind phospho serine/threonine motifs of numerous proteins (Mackintosh 2004). While different 14-3-3 proteins exhibit functional overlap, we show that ζ is the major isoform expressed in

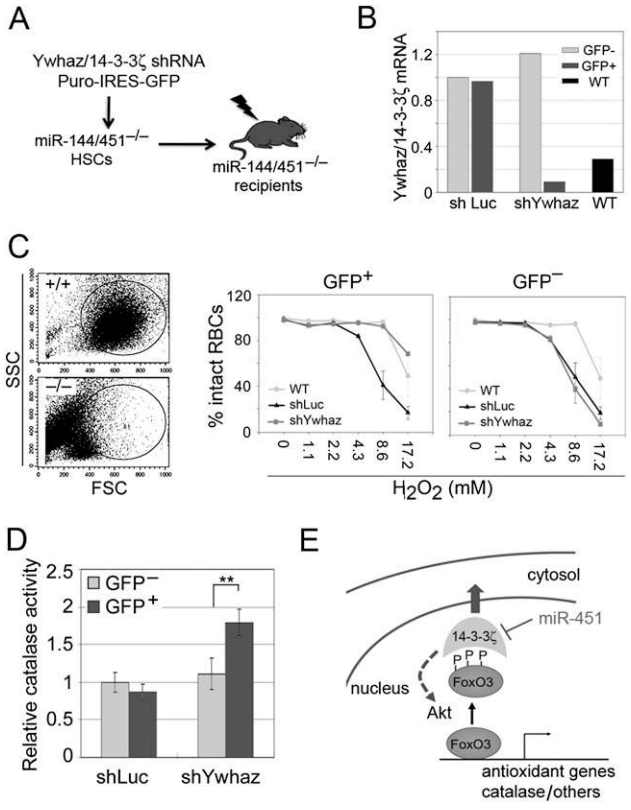

Figure 7. shRNA suppression of Ywhaz/14-3-3ζ in *miR-144/451*$^{-/-}$ erythrocytes alleviates susceptibility to oxidant stress. (*A*) *miR-144/451*$^{-/-}$ hematopoietic stem/progenitor cells were transduced with *Ywhaz/14-3-3ζ* shRNA-expressing retrovirus or luciferase (luc) shRNA virus as control and transplanted into lethally irradiated *miR-144/451*$^{-/-}$ recipient mice. The retroviral vector MSCV-PIG also expresses puromycin resistance and GFP expression cassettes. (*B*) Real-time RT–PCR comparing 14-3-3ζ mRNA in shRNA virus-infected (GFP$^+$) and uninfected (GFP$^-$) *miR-144/451*$^{-/-}$ bone marrow erythroblasts (CD71$^+$Ter119$^+$) from mice described in *A*. mRNA expression was normalized to 1.0 for GFP$^-$ cells from mice transplanted with shLuc-transduced bone marrow. (WT) CD71$^+$Ter119$^+$ erythroblasts from wild-type mice. A representative experiment from one mouse of each group is shown. (*C*) Ex vivo lysis of erythrocytes by H_2O_2. The far *left* panels show flow cytometry analysis of whole blood from *miR-144/451*$^{-/-}$ and wild-type (+/+) mice after treatment with 8.6 mM H_2O_2 for 3 h. Gating parameters for intact erythrocytes, determined by FSC and side scatter (SSC), are indicated. Mutant erythrocytes exhibit enhanced susceptibility to lysis, in agreement with the study described in Figure 1E. Sensitivity to H_2O_2-induced hemolysis was examined in whole blood of *miR-144/451*$^{-/-}$ recipient mice transplanted with shRNA-transduced *miR-144/451*$^{-/-}$ bone marrow. The graphs show fractions of intact GFP$^+$ (*middle* panel) and GFP$^-$ (*right* panel) erythrocytes after treatment with various concentrations H_2O_2. GFP$^-$ cells presumably derive from nontransduced mutant progenitors. As a control, results from nontransplanted wild-type mice are included. Three mice from each group were analyzed. (*D*) Relative catalase activities in flow cytometry-sorted GFP$^-$ and GFP$^+$ erythrocytes of transplanted mice. Catalase activity in GFP$^-$ cells from mice transplanted with shLuc-transduced bone marrow was normalized to an arbitrary value of 1. $n = 3$ mice from each group. (**) $P < 0.01$ (*t*-test). Representative results from one of three independent experiments are shown. (*E*) Model for miR-451 enhancement of FoxO3 activity via repression of 14-3-3ζ. The serine–threonine kinase AKT phosphorylates FoxO3, which then binds 14-3-3ζ to promote transport from nucleus to cytoplasm. 14-3-3ζ also stimulates AKT activation by promoting the formation of an upstream Shc–PI3 kinase signaling complex (not shown in the figure). miR-451 stimulates FoxO3 nuclear localization by directly repressing 14-3-3ζ mRNA.

miR-144/451$^{-/-}$ erythroid precursors (Fig. 5C,B; Supplemental Fig. 7). Thus, enhanced synthesis of 14-3-3ζ caused by loss of miR-451 induces a significant rise in total erythroid 14-3-3 activity, which partially inhibits FoxO3. *FoxO3*$^{-/-}$ mice exhibit relatively minor erythroid abnormalities at baseline, but are exquisitely sensitive to oxidant hemolysis (Marinkovic et al. 2007). The *miR-144/451*$^{-/-}$ erythroid phenotype is similar, although less severe, with only a subset of FoxO3-regulated transcripts dysregulated (Fig. 3C–F). This likely reflects partial attenuation of FoxO3 activity with distinct dosage thresholds for different target genes.

Previously, two groups (Dore et al. 2008; Du et al. 2009) observed that MO-induced miR-451 deficiency causes severe anemia in zebrafish embryos, while a third group (Pase et al. 2009) reported a milder phenotype resulting from similar experiments. Here we resolve this apparent discrepancy by showing that PTU, which was included specifically in our prior study (and presumably was also used by Du et al. 2009), synergizes with miR-451-MO to induce severe anemia via enhanced oxidant stress. Our findings that PTU can influence experimental results raise caution about its routine use to enhance transparency of zebrafish embryos, certainly in studies to investigate oxidant stress. Nonetheless, the effects of this drug observed in our current work indicate that the anti-oxidant activities of miR-451 are deeply conserved in evolution. In contrast, miR-451 targets transcription factor gata2 in zebrafish (Pase et al. 2009), while levels of the corresponding mRNA and protein are normal in murine *miR-144/451*$^{-/-}$ erythroblasts (data not shown). These findings are consistent with studies showing that, even while miRNAs and their general functions are commonly conserved throughout evolution, specific target genes frequently differ between species (Chen and Rajewsky 2007).

Our findings also raise new questions. Papapetrou et al. (2010) used lentivirus to express specific inhibitory miR-144 and miR-451 decoys to inhibit their activities in murine hematopoietic stem cells, and then studied their developmental potential after transplantation into irradiated mice. In these experiments, deficiency of either miRNA inhibited erythropoiesis to a significantly greater extent than we observed in *miR-144/451*$^{-/-}$ spleen or bone marrow. Several technical and biological explanations could explain this difference. For example, miRNA decoys may exert off-target effects by inhibiting additional miRNAs, although miR-144 or miR-451 homologs are not apparent in database searches. It is also possible that stresses associated with irradiation, bone marrow transplantation, and/or overexpression of ssRNAs somehow exacerbate the erythroid effects of decoy-mediated miR-144 and miR-451 deficiency, similar to what we observed for the combination of PTU and miR-451 MO in zebrafish. In any case, these contrasting results indicate that the biological effects of miRNA manipulation are highly influenced by experimental approaches, and that, in general, the greatest level of understanding requires multiple investigative modalities.

The miR-451–14-3-3ζ–FoxO3 regulatory axis identified here has potentially interesting and medically relevant implications beyond erythropoiesis. For example, a preliminary study reports that miR-451 confers resistance to ischemic and oxidant injuries in cardiomyocytes (Zhang 2009). As FoxO3 regulates anti-oxidant functions in the heart (Chiribau et al. 2008; Tan et al. 2008), miR-451 may protect against oxidant/hypoxic stresses through common mechanisms in cardiac and erythroid tissues. miR-451 is also expressed in various cancers, and is linked both positively and negatively to malignant progression and chemosensitivity (Gal et al. 2008; Kovalchuk et al. 2008; Bandres et al. 2009; Godlewski et al. 2010), reflecting the concept that miRNA actions are cell context-dependent. miR-451 is reported to both inhibit and promote growth of glioma cells (Gal et al. 2008; Kovalchuk et al. 2008). Down-regulation of miR-451 in gastric epithelial cancers is associated with decreased survival (Bandres et al. 2009). FoxO3 functions as a tumor suppressor, which inhibits mitosis and promotes apoptosis in specific cellular contexts (Yang and Hung 2009). Moreover, 14-3-3ζ is overexpressed in numerous cancers, where it regulates pathogenesis by inhibiting apoptosis induced by stress-activated kinase pathways or epithelial detachment from cellular basement membranes (anoikis) (Jang et al. 2004; Danes et al. 2008; Li et al. 2008; Niemantsverdriet et al. 2008). Accordingly, miR-451 may exert anti-oncogenic properties by suppressing 14-3-3ζ directly and/or indirectly activating FoxO3. In preliminary studies, we did not observe increased death rates in *miR-144/451*$^{-/-}$ mice of up to 1 yr of age. Thus, these miRNAs are not likely to represent potent tumor suppressors by themselves, at least in mice. Down-regulation of miR-451 may interact with other genetic aberrations to enhance or forestall the progression of different malignancies. It should now be possible to manipulate *miR-144/451*$^{-/-}$ mice to test the functions of this locus in nonerythroid tissues during stress and tumor formation.

Materials and methods

Animals and genotyping

A 388-base-pair segment of genomic DNA containing both the pre-miR-144 and pre-miR-451 regions was deleted by homologous recombination in embryonic stem cells (Supplemental Fig. 1A; Supplemental Material). The Institutional Animal Care and Use Committee of the Children's Hospital of Philadelphia approved all experiments.

Cells

G1E and G1E-ER4 erythroid cells were cultured as described (Gregory et al. 1999). NIH 3T3 cells were grown in DMEM supplemented with 10% serum and sodium pyruvate.

Antibodies

Flow cytometry antibodies were purchased from BD Biosciences: APC rat anti-mouse Ter119 (catalog no. 557909) and PE or FITC rat anti-mouse CD71 (catalog no. 553267 or 553266, respectively). For Western blots the following antibodies were used: HDAC2 (H-54, SC-7899, Santa Cruz Biotechnology), GAPDH (FL-385, SC-25778, Santa Cruz Biotechnology), PCNA (C-20,

SC-9857, Santa Cruz Biotechnology), 14-3-3ζ (C-16, SC-1019, Santa Cruz Biotechnology), Pan 14-3-3 (K-19, SC-629, Santa Cruz Biotechnology), 14-3-3ε (SC-130547, Santa Cruz Biotechnology), 14-3-3β (SC-628, Santa Cruz Biotechnology), 14-3-3η (SC-17286, Santa Cruz Biotechnology), AKT1-2-3 (H-136, SC-8312, Santa Cruz Biotechnology), p-AKT (Ser473, 587F11, Cell Signaling), Actin (clone AC-15, A3854, Sigma). Two different FoxO3 antibodies were used: 07-702 (Upstate Biotechnologies), a polyclonal antibody that recognizes an epitope corresponding to amino acids 330–673; and 75D8 (Cell Signaling), a monoclonal antibody that recognizes an epitope corresponding to amino acids around Glu50. Rabbit anti-mouse α-globin serum was prepared against full-length recombinant protein, and was used at a dilution of 1:5000 for Western blots.

Hematological studies

Complete blood counts were determined using the ADVIA 120 hematology analyzer. For PHZ treatment, 180 mg/kg 1-acetyl-2-PHZ (Sigma) was injected intraperitoneally on two consecutive days. Serial hematocrit levels were determined by standard methods after removing 15–20 μL of blood from the tail. Heinz body staining was performed as described (Stamatoyannopoulos et al. 1974). Methylcellulose colony assays were performed using standard methods. BFU-e cultures contained 2 U/mL human erythropoietin (Amgen), and 100 ng/mL SCF (R&D Systems). BSO (Sigma) was dissolved in water immediately before use and added to the cultures at the indicated concentrations before plating.

Measurement of ROS

Tail blood was collected into heparin-coated capillary tubes and transferred to microfuge tubes. Peripheral blood cells (10^7) were incubated with 10 μM 2′,7′-dichlorofluorescin (DCFH-DA; Invitrogen) for 20 min at 37°C, and were treated with H_2O_2 for another 20 min at 37°C. Fluorescence intensity was measured by flow cytometry.

H_2O_2-induced hemolysis

For the experiment in Figure 1E, erythrocytes were washed, resuspended at 2% packed cell volume in PBS with 20 mM glucose, and incubated for 12 h with H_2O_2 in a standard tissue culture incubator (37°C, 20% O_2, 5% CO_2). The cells were removed by centrifugation, and hemoglobin released into the supernatant was quantified by measuring light absorbance at 540 nm. One-hundred percent hemolysis was defined according to the amount of hemoglobin released after incubating the same concentration of erythrocytes with distilled water. To measure H_2O_2-induced lysis by flow cytometry (Fig. 7C), washed cells were incubated in H_2O_2 for 3 h, then FSC and side scatter were analyzed on GFP-gated cells using flow cytometry.

Catalase activity

Erythrocyte catalase activity was determined using the Catalase Assay Kit (Calbiochem) and normalized to hemoglobin concentration (OD_{570} nm) within cell lysates.

Zebrafish studies

Antisense MOs directed against zebrafish miR-451 (miRBase accession no. MIMAT0001634) were synthesized and injected into embryos as described previously (Dore et al. 2008). Zebrafish embryos were treated with 100 mM NAC and/or 1× PTU work solution (100× stock = 0.3% [w/v] for a final working solution of 0.003%).

Purification of Ter119$^+$ erythroid cells

Bone marrow and spleen erythroblasts were purified by magnetic sorting using the MACS-based separation system (Miltenyi Biotec). The enrichment, purity, and maturation stage of magnetic bead-purified cells were determined by analyzing the expression of Ter119 and CD71 surface antigens using flow cytometry.

Microarray analysis

CD71$^+$/Ter119$^+$/FSC-high bone marrow cells from *miR-144/451*$^{-/-}$ mice and wild-type controls were purified by flow cytometry and deposited directly into Trizol LS reagent (Invitrogen). Samples were processed for microarray analysis using the GeneChip Mouse Genome 430 2.0 Array (Affymetrix, Inc.) by the microarray core facility at the University of Pennsylvania, and were analyzed as described in Supplemental Material. Raw microarray findings are deposited in Gene Expression Omnibus (GEO), accession number GSE21041.

Enforced expression of miRNAs and 14-3-3ζ

Construction of retroviral expression vectors, transduction of cells, and Northern blots are described in the Supplemental Material.

Image analysis of FoxO3 expression

Confocal microscopy and ImageStream analysis are described in the Supplemental Material.

Bone marrow transplantation

Bone marrow cells were harvested from *miR-144/451*$^{-/-}$ mice (C57BL/6J), and were lineage-depleted with biotinylated rat anti-mouse antibodies including Ter119, Gr1, Mac1, B220, CD19, IL-7R, CD4, CD8, and CD5 (eBioscience), and Dynal sheep anti-rat magnetic beads (Invitrogen, SKU#110-35). The Lin (−) cells were cultured in DMEM containing IL-3, IL-6, and SCF cytokines, and were infected twice with PIG-shLuc or PIG-shYwhaz/14-3-3ζ virus (Hemann et al. 2003). On day 2, the cells were washed with PBS and 2×10^5 cells were injected retro-orbitally into 8- to 12-wk-old *miR-144/451*$^{-/-}$ recipient mice that were irradiated previously with 10 Gy in two split doses of 5 Gy, 4 h apart.

Acknowledgments

We thank Marike von Lindern for providing microarray data and discussion. We thank Morrie Birnbaum and Andrei Thomas-Tikhonenko for helpful suggestions. We are grateful to Bruce Shenker and Ali Zekavat for providing access to the Amnis ImageStream flow cytometer, and Janine Lamonica for providing puromycin-sensitive G1E-ER cells. We thank Karen Kim, Eric Valentine, and Xiang Yu for technical assistance. This work was funded by a grant from the Roche Foundation for Anemia Research (M.J.W.), March of Dimes Foundation (B.H.P.), and The National Institutes of Health (R01 DK070838, P01 HL032262, and P30 DK072437 to B.H.P., and R01 AI067946 to J.S.O.).

References

Ambros V. 2008. The evolution of our thinking about microRNAs. *Nat Med* **14:** 1036–1040.

Bakker WJ, Blazquez-Domingo M, Kolbus A, Besooyen J, Steinlein P, Beug H, Coffer PJ, Lowenberg B, von Lindern M, van Dijk TB. 2004. FoxO3a regulates erythroid differentiation and

induces BTG1, an activator of protein arginine methyl transferase 1. *J Cell Biol* **164:** 175–184.
Bakker WJ, van Dijk TB, Parren-van Amelsvoort M, Kolbus A, Yamamoto K, Steinlein P, Verhaak RG, Mak TW, Beug H, Lowenberg B, et al. 2007. Differential regulation of Foxo3a target genes in erythropoiesis. *Mol Cell Biol* **27:** 3839–3854.
Bandres E, Bitarte N, Arias F, Agorreta J, Fortes P, Agirre X, Zarate R, Diaz-Gonzalez JA, Ramirez N, Sola JJ, et al. 2009. microRNA-451 regulates macrophage migration inhibitory factor production and proliferation of gastrointestinal cancer cells. *Clin Cancer Res* **15:** 2281–2290.
Barry EF, Felquer FA, Powell JA, Biggs L, Stomski FC, Urbani A, Ramshaw H, Hoffmann P, Wilce MC, Grimbaldeston MA, et al. 2009. 14-3-3:Shc scaffolds integrate phosphoserine and phosphotyrosine signaling to regulate phosphatidylinositol 3-kinase activation and cell survival. *J Biol Chem* **284:** 12080–12090.
Bartel DP. 2004. MicroRNAs: Genomics, biogenesis, mechanism, and function. *Cell* **116:** 281–297.
Bonfigli A, Zarivi O, Colafarina S, Cimini AM, Ragnelli AM, Aimola P, Natali PG, Ceru MP, Amicarelli F, Miranda M. 2006. Human glioblastoma ADF cells express tyrosinase, L-tyrosine hydroxylase and melanosomes and are sensitive to L-tyrosine and phenylthiourea. *J Cell Physiol* **207:** 675–682.
Bruchova H, Yoon D, Agarwal AM, Mendell J, Prchal JT. 2007. Regulated expression of microRNAs in normal and polycythemia vera erythropoiesis. *Exp Hematol* **35:** 1657–1667.
Brummer T, Larance M, Herrera Abreu MT, Lyons RJ, Timpson P, Emmerich CH, Fleuren ED, Lehrbach GM, Schramek D, Guilhaus M, et al. 2008. Phosphorylation-dependent binding of 14-3-3 terminates signalling by the Gab2 docking protein. *EMBO J* **27:** 2305–2316.
Brunet A, Bonni A, Zigmond MJ, Lin MZ, Juo P, Hu LS, Anderson MJ, Arden KC, Blenis J, Greenberg ME. 1999. Akt promotes cell survival by phosphorylating and inhibiting a Forkhead transcription factor. *Cell* **96:** 857–868.
Calnan DR, Brunet A. 2008. The FoxO code. *Oncogene* **27:** 2276–2288.
Carthew RW, Sontheimer EJ. 2009. Origins and mechanisms of miRNAs and siRNAs. *Cell* **136:** 642–655.
Cheloufi S, Dos Santos CO, Chong MM, Hannon GJ. 2010. A dicer-independent miRNA biogenesis pathway that requires Ago catalysis. *Nature* **465:** 584–589.
Chen K, Rajewsky N. 2007. The evolution of gene regulation by transcription factors and microRNAs. *Nat Rev Genet* **8:** 93–103.
Chiribau CB, Cheng L, Cucoranu IC, Yu YS, Clempus RE, Sorescu D. 2008. FOXO3A regulates peroxiredoxin III expression in human cardiac fibroblasts. *J Biol Chem* **283:** 8211–8217.
Choong ML, Yang HH, McNiece I. 2007. MicroRNA expression profiling during human cord blood-derived CD34 cell erythropoiesis. *Exp Hematol* **35:** 551–564.
Cifuentes D, Xue H, Taylor DW, Patnode H, Mishima Y, Cheloufi S, Ma E, Mane S, Hannon GJ, Lawson N, et al. 2010. A novel miRNA processing pathway independent of Dicer requires Argonaute2 catalytic activity. *Science* . **328:** 1694–1698
Danes CG, Wyszomierski SL, Lu J, Neal CL, Yang W, Yu D. 2008. 14-3-3ζ down-regulates p53 in mammary epithelial cells and confers luminal filling. *Cancer Res* **68:** 1760–1767.
Das K, Chainy GB. 2004. Thyroid hormone influences antioxidant defense system in adult rat brain. *Neurochem Res* **29:** 1755–1766.
Dennis G Jr, Sherman BT, Hosack DA, Yang J, Gao W, Lane HC, Lempicki RA. 2003. DAVID: Database for annotation, visualization, and integrated discovery. *Genome Biol* **4:** R60. doi: 10.1186/gb-2003-4-9-r60.
Dore LC, Amigo JD, Dos Santos CO, Zhang Z, Gai X, Tobias JW, Yu D, Klein AM, Dorman C, Wu W, et al. 2008. A GATA-1-regulated microRNA locus essential for erythropoiesis. *Proc Natl Acad Sci* **105:** 3333–3338.
Du TT, Fu YF, Dong M, Wang L, Fan HB, Chen Y, Jin Y, Chen SJ, Chen Z, Deng M, et al. 2009. Experimental validation and complexity of miRNA-mRNA target interaction during zebrafish primitive erythropoiesis. *Biochem Biophys Res Commun* **381:** 688–693.
Felli N, Fontana L, Pelosi E, Botta R, Bonci D, Facchiano F, Liuzzi F, Lulli V, Morsilli O, Santoro S, et al. 2005. MicroRNAs 221 and 222 inhibit normal erythropoiesis and erythroleukemic cell growth via kit receptor down-modulation. *Proc Natl Acad Sci* **102:** 18081–18086.
Flynt AS, Lai EC. 2008. Biological principles of microRNA-mediated regulation: Shared themes amid diversity. *Nat Rev Genet* **9:** 831–842.
Fu YF, Du TT, Dong M, Zhu KY, Jing CB, Zhang Y, Wang L, Fan HB, Chen Y, Jin Y, et al. 2009. mir-144 selectively regulates embryonic α-hemoglobin synthesis during primitive erythropoiesis. *Blood*. **113:** 1340–1349
Gal H, Pandi G, Kanner AA, Ram Z, Lithwick-Yanai G, Amariglio N, Rechavi G, Givol D. 2008. MIR-451 and Imatinib mesylate inhibit tumor growth of Glioblastoma stem cells. *Biochem Biophys Res Commun* **376:** 86–90.
George TC, Fanning SL, Fitzgerald-Bocarsly P, Medeiros RB, Highfill S, Shimizu Y, Hall BE, Frost K, Basiji D, Ortyn WE, et al. 2006. Quantitative measurement of nuclear translocation events using similarity analysis of multispectral cellular images obtained in flow. *J Immunol Methods* **311:** 117–129.
Godlewski J, Nowicki MO, Bronisz A, Nuovo G, Palatini J, De Lay M, Van Brocklyn J, Ostrowski MC, Chiocca EA, Lawler SE. 2010. MicroRNA-451 regulates LKB1/AMPK signaling and allows adaptation to metabolic stress in glioma cells. *Mol Cell* **37:** 620–632.
Gregory T, Yu C, Ma A, Orkin SH, Blobel GA, Weiss MJ. 1999. GATA-1 and erythropoietin cooperate to promote erythroid cell survival by regulating bcl-xL expression. *Blood* **94:** 87–96.
Hemann MT, Fridman JS, Zilfou JT, Hernando E, Paddison PJ, Cordon-Cardo C, Hannon GJ, Lowe SW. 2003. An epi-allelic series of p53 hypomorphs created by stable RNAi produces distinct tumor phenotypes in vivo. *Nat Genet* **33:** 396–400.
Huang H, Tindall DJ. 2007. Dynamic FoxO transcription factors. *J Cell Sci* **120:** 2479–2487.
Jang JS, Cho HY, Lee YJ, Ha WS, Kim HW. 2004. The differential proteome profile of stomach cancer: Identification of the biomarker candidates. *Oncol Res* **14:** 491–499.
Karlsson J, von Hofsten J, Olsson PE. 2001. Generating transparent zebrafish: A refined method to improve detection of gene expression during embryonic development. *Mar Biotechnol (NY)* **3:** 522–527.
Kloosterman WP, Steiner FA, Berezikov E, de Bruijn E, van de Belt J, Verheul M, Cuppen E, Plasterk RH. 2006. Cloning and expression of new microRNAs from zebrafish. *Nucleic Acids Res* **34:** 2558–2569.
Kops GJ, Dansen TB, Polderman PE, Saarloos I, Wirtz KW, Coffer PJ, Huang TT, Bos JL, Medema RH, Burgering BM. 2002. Forkhead transcription factor FOXO3a protects quiescent cells from oxidative stress. *Nature* **419:** 316–321.
Kovalchuk O, Filkowski J, Meservy J, Ilnytskyy Y, Tryndyak VP, Chekhun VF, Pogribny IP. 2008. Involvement of microRNA-451 in resistance of the MCF-7 breast cancer cells to chemotherapeutic drug doxorubicin. *Mol Cancer Ther* **7:** 2152–2159.

Lewis BP, Burge CB, Bartel DP. 2005. Conserved seed pairing, often flanked by adenosines, indicates that thousands of human genes are microRNA targets. *Cell* **120:** 15–20.

Li QJ, Chau J, Ebert PJ, Sylvester G, Min H, Liu G, Braich R, Manoharan M, Soutschek J, Skare P, et al. 2007. miR-181a is an intrinsic modulator of T cell sensitivity and selection. *Cell* **129:** 147–161.

Li Z, Zhao J, Du Y, Park HR, Sun SY, Bernal-Mizrachi L, Aitken A, Khuri FR, Fu H. 2008. Down-regulation of 14-3-3ζ suppresses anchorage-independent growth of lung cancer cells through anoikis activation. *Proc Natl Acad Sci* **105:** 162–167.

Lim LP, Lau NC, Garrett-Engele P, Grimson A, Schelter JM, Castle J, Bartel DP, Linsley PS, Johnson JM. 2005. Microarray analysis shows that some microRNAs downregulate large numbers of target mRNAs. *Nature* **433:** 769–773.

Liu Y, Pop R, Sadegh C, Brugnara C, Haase VH, Socolovsky M. 2006. Suppression of Fas–FasL coexpression by erythropoietin mediates erythroblast expansion during the erythropoietic stress response in vivo. *Blood* **108:** 123–133.

Mackintosh C. 2004. Dynamic interactions between 14-3-3 proteins and phosphoproteins regulate diverse cellular processes. *Biochem J* **381:** 329–342.

Marinkovic D, Zhang X, Yalcin S, Luciano JP, Brugnara C, Huber T, Ghaffari S. 2007. Foxo3 is required for the regulation of oxidative stress in erythropoiesis. *J Clin Invest* **117:** 2133–2144.

Masaki S, Ohtsuka R, Abe Y, Muta K, Umemura T. 2007. Expression patterns of microRNAs 155 and 451 during normal human erythropoiesis. *Biochem Biophys Res Commun* **364:** 509–514.

Merkerova M, Belickova M, Bruchova H. 2008. Differential expression of microRNAs in hematopoietic cell lineages. *Eur J Haematol* **81:** 304–310.

Nemoto S, Finkel T. 2002. Redox regulation of forkhead proteins through a p66shc-dependent signaling pathway. *Science* **295:** 2450–2452.

Niemantsverdriet M, Wagner K, Visser M, Backendorf C. 2008. Cellular functions of 14-3-3ζ in apoptosis and cell adhesion emphasize its oncogenic character. *Oncogene* **27:** 1315–1319.

O'Carroll D, Mecklenbrauker I, Das PP, Santana A, Koenig U, Enright AJ, Miska EA, Tarakhovsky A. 2007. A Slicer-independent role for Argonaute 2 in hematopoiesis and the microRNA pathway. *Genes Dev* **21:** 1999–2004.

Papapetrou EP, Korkola JE, Sadelain M. 2010. A genetic strategy for single and combinatorial analysis of miRNA function in mammalian hematopoietic stem cells. *Stem Cells*. **28:** 287–296

Pase L, Layton JE, Kloosterman WP, Carradice D, Waterhouse PM, Lieschke GJ. 2009. miR-451 regulates zebrafish erythroid maturation in vivo via its target gata2. *Blood*. **113:** 1794–1804

Patrick DM, Zhang CC, Tao Y, Yao H, Qi X, Schwartz RJ, Huang LJ-S,Olson EN. 2010. Defective erythroid differentiation in miR-451 mutant mice mediated by 14-3-3ζ. *Genes Dev* (this issue). doi: 10.1101/gad.1942810.

Rathjen T, Nicol C, McConkey G, Dalmay T. 2006. Analysis of short RNAs in the malaria parasite and its red blood cell host. *FEBS Lett* **580:** 5185–5188.

Socolovsky M, Nam H, Fleming MD, Haase VH, Brugnara C, Lodish HF. 2001. Ineffective erythropoiesis in Stat5a$^{-/-}$5b$^{-/-}$ mice due to decreased survival of early erythroblasts. *Blood* **98:** 3261–3273.

Stamatoyannopoulos G, Woodson R, Papayannopoulou T, Heywood D, Kurachi S. 1974. Inclusion-body β-thalassemia trait. A form of β thalassemia producing clinical manifestations in simple heterozygotes. *N Engl J Med* **290:** 939–943.

Stomski FC, Dottore M, Winnall W, Guthridge MA, Woodcock J, Bagley CJ, Thomas DT, Andrews RK, Berndt MC, Lopez AF. 1999. Identification of a 14-3-3 binding sequence in the common β chain of the granulocyte-macrophage colony-stimulating factor (GM-CSF), interleukin-3 (IL-3), and IL-5 receptors that is serine-phosphorylated by GM-CSF. *Blood* **94:** 1933–1942.

Tan WQ, Wang K, Lv DY, Li PF. 2008. Foxo3a inhibits cardiomyocyte hypertrophy through transactivating catalase. *J Biol Chem* **283:** 29730–29739.

van Rooij E, Sutherland LB, Qi X, Richardson JA, Hill J, Olson EN. 2007. Control of stress-dependent cardiac growth and gene expression by a microRNA. *Science* **316:** 575–579.

Wang WD, Wang Y, Wen HJ, Buhler DR, Hu CH. 2004. Phenylthiourea as a weak activator of aryl hydrocarbon receptor inhibiting 2,3,7,8-tetrachlorodibenzo-p-dioxin-induced CYP1A1 transcription in zebrafish embryo. *Biochem Pharmacol* **68:** 63–71.

Wang Q, Huang Z, Xue H, Jin C, Ju XL, Han JD, Chen YG. 2008. MicroRNA miR-24 inhibits erythropoiesis by targeting activin type I receptor ALK4. *Blood* **111:** 588–595.

Welch JJ, Watts JA, Vakoc CR, Yao Y, Wang H, Hardison RC, Blobel GA, Chodosh LA, Weiss MJ. 2004. Global regulation of erythroid gene expression by transcription factor GATA-1. *Blood* **104:** 3136–3147.

Williams AH, Valdez G, Moresi V, Qi X, McAnally J, Elliott JL, Bassel-Duby R, Sanes JR, Olson EN. 2009. MicroRNA-206 delays ALS progression and promotes regeneration of neuromuscular synapses in mice. *Science* **326:** 1549–1554.

Wu JP, Chang LW, Yao HT, Chang H, Tsai HT, Tsai MH, Yeh TK, Lin P. 2009. Involvement of oxidative stress and activation of aryl hydrocarbon receptor in elevation of CYP1A1 expression and activity in lung cells and tissues by arsenic: An in vitro and in vivo study. *Toxicol Sci.* **107:** 385–393

Yang JY, Hung MC. 2009. A new fork for clinical application: Targeting forkhead transcription factors in cancer. *Clin Cancer Res* **15:** 752–757.

Zamoner A, Barreto KP, Filho DW, Sell F, Woehl VM, Guma FC, Pessoa-Pureur R, Silva FR. 2008. Propylthiouracil-induced congenital hypothyroidism upregulates vimentin phosphorylation and depletes antioxidant defenses in immature rat testis. *J Mol Endocrinol* **40:** 125–135.

Zhan M, Miller CP, Papayannopoulou T, Stamatoyannopoulos G, Song CZ. 2007. MicroRNA expression dynamics during murine and human erythroid differentiation. *Exp Hematol* **35:** 1015–1025.

Zhang PC, Chen J, Ren X, Wang X, Kranias EG, Medvedovic M, Fan G-C. 2009. MicroRNA expression profiling in the ischemic preconditioned heart: Functional role of a miR-1/GATA-4/miR-144, -451, and -762 circuit. *Circulation* **120:** S736.

miR-451 protects against erythroid oxidant stress by repressing 14-3-3 ζ

Duonan Yu, Camila O. dos Santos, Guowei Zhao, et al.

Genes Dev. 2010, **24:**
Access the most recent version at doi:10.1101/gad.1942110